Applied Physics Letters

Tunable auxetic metamaterials for simultaneous attenuation of airborne sound and elastic vibrations in all directions 🅕 🆂🅲🅸

🆔 Majid Kheybari, 🆔 Chiara Daraio and 🆔 Osama R. Bilal

COLLECTIONS

Paper published as part of the special topic on Acoustic and Elastic Metamaterials and Metasurfaces

🅕 This paper was selected as Featured

🆂🅲🅸 This paper was selected as Scilight

View Online   Export Citation   CrossMark

ARTICLES YOU MAY BE INTERESTED IN

Inertially amplified seismic metamaterial with an ultra-low-frequency bandgap
Applied Physics Letters **121**, 081701 (2022); https://doi.org/10.1063/5.0102821

'A quieter world'
Scilight **2022**, 351104 (2022); https://doi.org/10.1063/10.0013891

Mode hybridization in DNA-inspired helical metamaterials with variable centro-asymmetry
Applied Physics Letters **121**, 072201 (2022); https://doi.org/10.1063/5.0106740

APL Quantum
CALL FOR APPLICANTS
Seeking Editor-in-Chief

AIP Publishing

Tunable auxetic metamaterials for simultaneous attenuation of airborne sound and elastic vibrations in all directions

Majid Kheybari,[1] (iD) Chiara Daraio,[2] (iD) and Osama R. Bilal[1,a)] (iD)

AFFILIATIONS

[1]Department of Mechanical Engineering, University of Connecticut, Storrs, Connecticut 06269, USA
[2]Department of Mechanical and Civil Engineering, California Institute of Technology, Pasadena, California 91125, USA

Note: This paper is part of the APL Special Collection on Acoustic and Elastic Metamaterials and Metasurfaces.
[a)]Author to whom correspondence should be addressed: osama.bilal@uconn.edu

ABSTRACT

Through a combination of analytical, numerical, and experimental methods, we study a three-dimensional metamaterial with the ability to attenuate both airborne sound and mechanical vibrations, simultaneously, and in all directions. In addition, due to the auxetic nature of the design (i.e., having a negative Poisson's ratio), the metamaterial can shrink (or expand) in a relatively uniform manner, without buckling. We utilize an external load to cause a systematic shape change in the metamaterial and tune the attenuation frequency bands. The presented design principles can be utilized in many applications related to acoustic and elastic wave manipulation as well as acoustic devices.

Published under an exclusive license by AIP Publishing. https://doi.org/10.1063/5.0104266

Metamaterials are arrangements of basic building blocks (i.e., unit cell) that repeat in space, giving rise to intriguing properties, such as polar elasticity,[1] non-reciprocity,[2] and negative effective properties (Poisson's ratio,[3] mass-density,[4,5] and stiffness[6,7]), which are rare or not possible for conventional materials. The literature of metamaterials with remarkable properties can be loosely classified into three broad categories of (1) mechanical metamaterials that display unusual quasi-static performance such as resistance to shear,[8,9] indentation,[10] fracture,[11] and energy absorption;[12] (2) acoustic metamaterials that can manipulate a sound wave propagating within a fluid medium; or (3) elastic metamaterials, which have the ability to control vibrations within a solid domain.[13] An intriguing direction in the design of metamaterials is the integration of multiple functionalities at once, bringing the field closer to practical applications. For example, metamaterials that can manipulate both airborne sound and mechanical vibrations[13–18] or metamaterials with combined quasi-static and dynamic properties.[19,20] Metamaterials have been proposed for potential applications in the automotive sector,[21] sensors,[22] biomedical devices,[23] textiles,[24] sound insulation,[25–28] wave-guiding,[29,30] focusing,[31] and cloaking.[32]

In this study, we present an anisotropic auxetic (i.e., with a negative Poisson's ratio) metamaterial that can attenuate both elastic vibrations and airborne sound waves, simultaneously, and in all directions [Fig. 1(a)]. In addition, the attenuation frequency ranges (i.e., band gaps)

for both acoustic and elastic waves can be tuned (i.e., either widened or vanished) by applying an external quasi-static load to the metamaterial [Fig. 1(b)]. The design methodology is based on two attributes: (1) air-chambers connected by narrow slits to control airborne sound and (2) elastic regions connected by thinner features to control mechanical vibrations.[13] Both design attributes are included within a reentrant unit cell frame, to ensure auxetic behavior and allow for tunability.

We start our analysis by considering the dynamics of a metamaterial unit cell that repeats infinitely in space. We utilize the finite element method, using COMSOL Multi-physics (5.4), to analyze the metamaterials. The unit cell dimensions are $a_x = a_y = 24$(mm) and $a_z = 20$(mm). We implement Bloch solution in the form: $\mathbf{u}(\mathbf{x}, \kappa; t) = \tilde{\mathbf{u}}(\mathbf{x}, \kappa)e^{i(\kappa.\mathbf{x}-\omega t)}$, where $\tilde{\mathbf{u}}$ is the Bloch displacement vector, κ is the wave number, t is time, $\mathbf{x}$ is the position vector, and ω is the frequency. By employing Bloch solution, we can solve the system's equations of motion as an eigenvalue problem in the form: $[-\omega^2\mathbf{M} + \mathbf{K}(\kappa)]\boldsymbol{u} = 0$, where $\mathbf{M}$ and $\mathbf{K}$ are the discretized mass and stiffness matrices using the finite element method. We calculate the unit cell's dispersion curves for both wave types: elastic vibrations within the solid [Fig. 2(a)] and airborne sound within the surrounding air [Fig. 2(b)]. Both dispersion curves show a complete bandgap (highlighted in gray) along the high symmetry path $\Gamma - X - M - \Gamma - Z - R - A - \Gamma$ [Fig. 2(b), inset]. The symmetry points used are a result of the rectangular shape of the
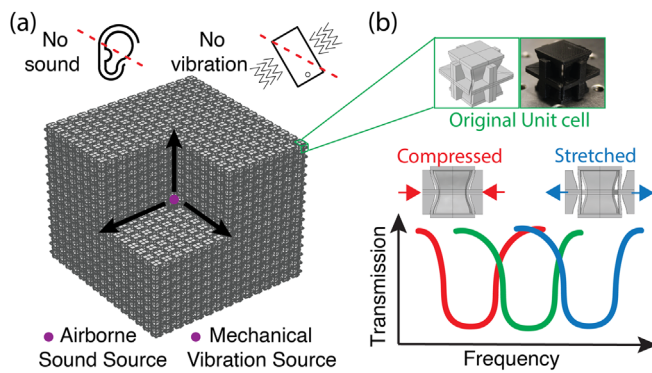
FIG. 1. Concept: (a) Auxetic vibro-acoustic metamaterial can attenuate both elastic and acoustic waves. (b) By applying an external load to the metamaterial, we can tune the attenuation frequency range for both airborne sound and mechanical vibrations, in all directions.
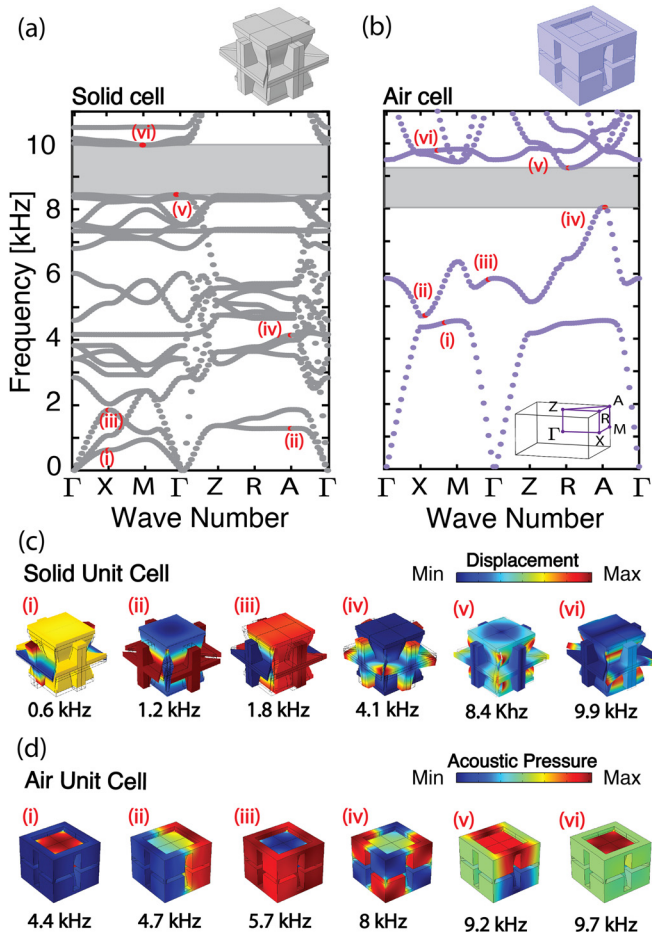
unit cell (i.e., in contrast to a simpler cubic unit cell).[33] Figure 2(c) shows six different vibrational mode shapes of the solid unit cell highlighting (i) an out-of-plane seesaw movement of the plus-sign side panel of the unit cell, (ii) an auxetic mode (all sides are expanding and contraction in phase), (iii) a longitudinal mode, (iv) rotational mode of the plus-sign panels, in addition to the two modes at the edge of the bandgap (v) and (vi). Figure 2(d) shows six different vibrational mode shapes of the air unit cell highlighting (i) and (vi) resonances of the inside cube, (ii) a dipole resonance mode, (iii) a resonance mode of the outside cube, (iv) an octopole mode, and a dipole mode (v).

Due to the embedded reentrant frame within the unit cell design, an applied load, either in compression or tension, induces a systematic change in the unit cell geometry. In other words, the unit cell expands or shrinks as a whole under external load, preserving most of its features. We capitalize on such systemic change in shape to tune the attenuation region of the metamaterials. We consider the unit cell under no external load as our baseline with a complete bandgap between 8 and 9.2 kHz for acoustic waves and between 8.4 and 9.9 kHz for elastic waves, in all directions. First, we apply a prescribed displacement on the unit cell sides in both x- and y-directions and compute the deformation of the unit cell sides in the z-direction.

FIG. 2. Unit cell analysis. Dispersion curves of the auxetic metamaterial for (a) mechanical vibrations and (b) airborne sound (bandgap regions are highlighted in gray). (c) Elastic and (d) acoustic mode shapes of the corresponding unit cell at select frequencies.
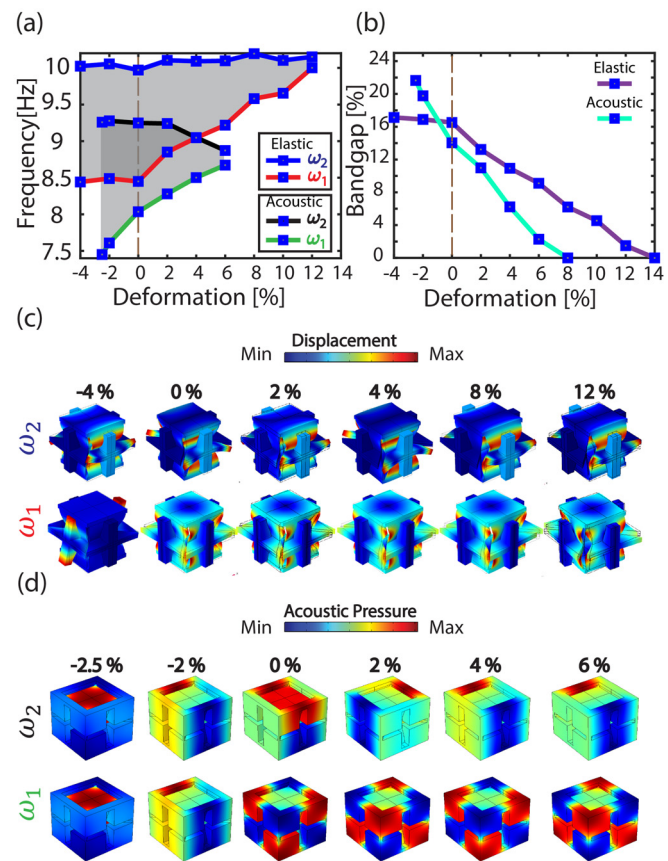

FIG. 3. Band gap tuning. Change in the upper and lower bandgap frequency range as a function of deformation (%). (b) Relative bandgap size as a function of deformation (%). The upper and lower frequency mode shapes of the (c) solid unit cell and (d) air unit cell.

Then, we calculate a new dispersion curves for the emerging unit cell (with an updated lattice constant in *x*, *y*, and *z*), while taking into account the internal stresses that accumulates within the unit cell. We track the evolution of the bandgap frequency range (i.e., both lower and upper edge of the bandgap) as a function of the applied load [Fig. 3(a)]. We also calculate the relative width of the bandgap [Fig. 3(b)] as $BG\% = (\omega_1 - \omega_2)/[(\omega_1 + \omega_2)/2]$, where ω_1 and ω_2 are the lower and upper frequency bounds of the bandgap, respectively. As the unit cell gets stretched outwards, the bandgap frequency range shrinks, until it vanishes at $8\%a_x$ deformation for acoustic waves and $14\%a_x$ deformation for elastic waves. In contrast, compressing the unit cell increases the bandgap frequency range for acoustic waves and has a minute effect on elastic waves (see the supplementary material for all dispersion curves for both wave types under external applied loads). The mode shapes for different $\omega(s)$ are plotted in Figs. 3(c) and 3(d).

To validate the unit cell model (i.e., with infinite periodicity), we consider a structural level analysis of the metamaterial (i.e., finite model). We tessellate the unit cell (both solid and air, separately) in a $7 \times 7 \times 7$ cuboid [Figs. 4(b) and 4(e)]. We apply a harmonic excitation at the surface of the cuboid, shown as black (x-direction), red (y-direction), and blue (z-direction) markers in Figs. 4(b) and 4(e). We sweep through frequencies between 1 Hz and 11 kHz and record the response amplitude at the opposite surface of the excitation point. The transmission results show clear attenuation through the solid and air cubes at the predicted bandgap regions as highlighted in gray in Figs. 4(a) and 4(d). To visualize the transmission and attenuation of exited waves within the metamaterial, we superimpose the response amplitude as heat maps over the finite sample when excited at 4.5 and 9 kHz for both wave types in all directions [Figs. 4(c) and 4(f)].

At 4.5 kHz, a passband frequency, elastic waves propagate throughout the structure when excited in any of the three principle axes x, y, or z. However, at 9 kHz, elastic waves are attenuated in all directions. It is worth noting that the wave is immediately attenuated when excited in the z-direction, while there exists a line-like surface mode for both x and y excitations. At 4.5 kHz, which is also a passband frequency for airborne sound, the wave propagates freely within the lattice regardless of excitation direction [Fig. 4(f), top]. At 9 kHz, a stop band frequency exists for airborne sound as well, the wave is not allowed to propagate through the medium [Fig. 4(f), bottom].

To validate our numerical simulations of the infinite and finite structures, we fabricate a $3 \times 3 \times 3$ cuboid using additive manufacturing (3D printer Fromlabs 3) (Fig. 5). We characterize the material properties in-house using a dog-bone tension test (see the supplementary material). The measured material properties are Young's modulus $E = 1.22$ GPa, density $\rho = 1205$ kg/m^3, and Poisson's ratio $\nu = 0.3$. We experimentally test the sample by mounting it on top of a mechanical shaker (Brüel and Kjær 4180) [Fig. 5(a)] and harmonically sweep through frequencies from 1 to 11 kHz. We measure the metamaterial response using a scanning laser Doppler vibrometer (Polytech-PSV-500). We replicate the experiment numerically and plot the response of both the numerical and experimental transmission as a function of frequency [Fig. 5(b)]. The predicted bandgap frequency range (highlighted in gray) using the infinite unit cell model matches well with the numerical transmission. The experimental transmission at 0% compression matches fairly with the predicted frequency range. The discrepancy might stem from manufacturing tolerances or the small number of unit cells. To experimentally validate the tunability of the transmission, we compress a $3 \times 3 \times 3$ cuboid (see supplementary material, Fig. S5)
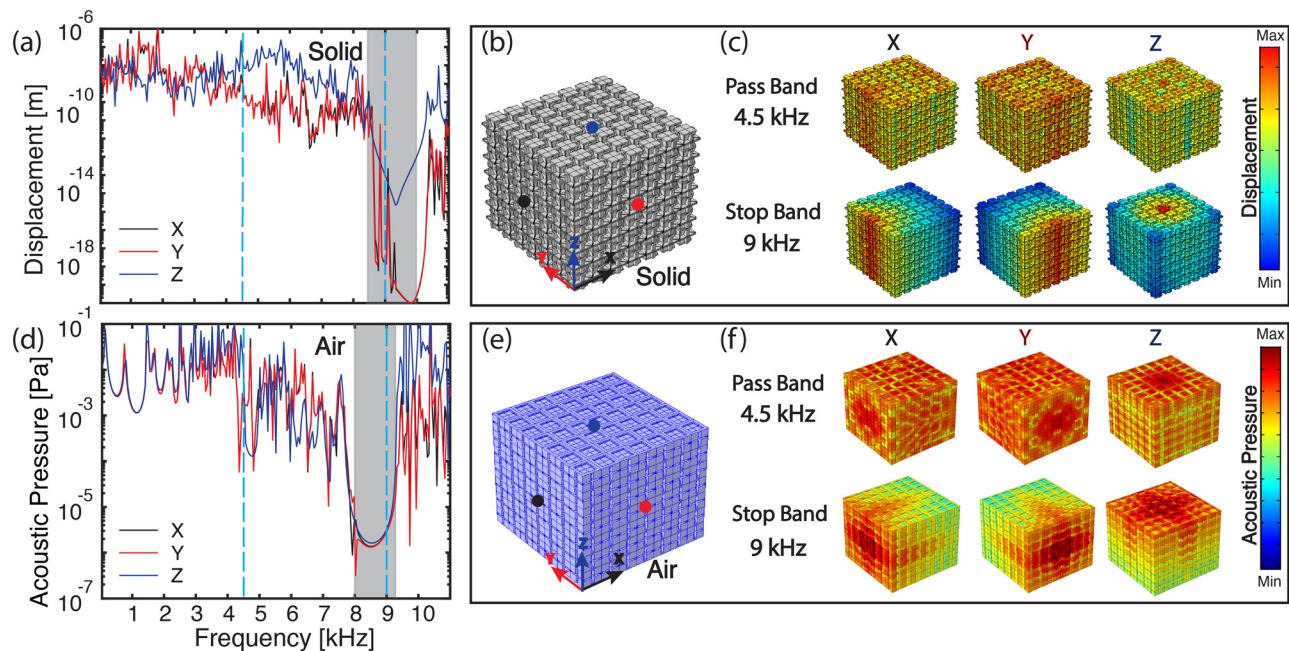

FIG. 4. Finite structure analysis. Frequency response functions of (a) finite solid cube and (d) finite air cube. The bandgap regions are highlighted in gray. Excitation points are marked with circles on the (b) solid and (e) air cubes. (c) Displacement heat maps of the solid cube at 4.5 kHz, a passband frequency (top) and 9 kHz, a stop band frequency (bottom). (f) Acoustic pressure heat maps of the air cube at 4.5 kHz, a passband frequency (top) and 9 kHz, a stop band frequency (bottom).
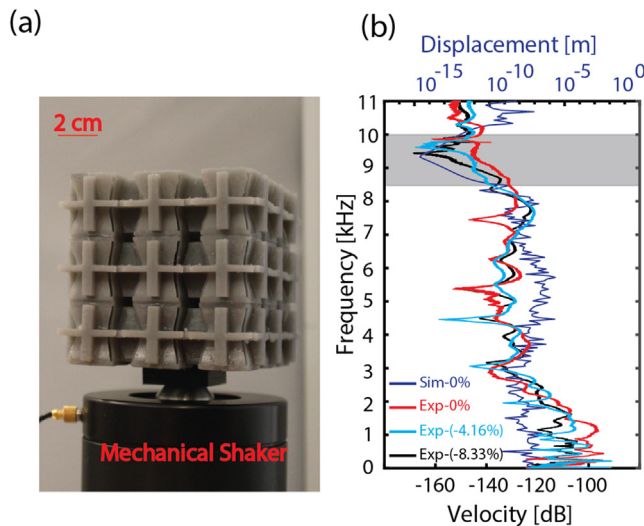
FIG. 5. Experimental measurement. (a) A finite metamaterial sample mounted on a mechanical shaker. (b) Experimental frequency response function of sample having 0%, −4.16%, and −8.33% deformation vs numerical frequency response functions at 0% deformation. Analytically predicted bandgap region is highlighted in gray.

in both x- and y-directions, simultaneously, with $-4.16\% a_x$ and $-8.33\% a_x$ and observe the transmission through the sample [Fig. 4(b)]. As predicted, the bandgap still exists, even after $-8\% a$ compression.

In this study, we present a design methodology, simulations, and experiments of an auxetic, anisotropic metamaterial that can simultaneously attenuate both elastic vibrations and airborne sound in all directions. Due to the auxetic nature of the metamaterial, an applied load, either in compression or tension, causes a systematic shape change within the unit cell. The resulting transformation in geometry induces a shift in the attenuated frequency ranges for both sound and vibrations, independently. Our results can open new avenues for the design of tunable multi-functional metamaterials, with potential application in vibration and sound control.

See the supplementary material for more information about the material's properties, unit cell feature sizes, effect of Poisson's ratio, dispersion curve evolution, and experimental methods.

AUTHOR DECLARATIONS
Conflict of Interest

The authors have no conflicts to disclose.

Author Contributions

Majid Kheybari: Data curation (equal); Formal analysis (equal); Investigation (equal); Software (equal); Validation (equal); Visualization (equal); Writing – original draft (equal); Writing – review and editing (equal). **Chiara Daraio:** Supervision (equal). **Osama R. Bilal:** Conceptualization (equal); Data curation (equal); Formal analysis (equal); Funding acquisition (equal); Investigation (equal); Methodology (equal); Project administration (equal); Supervision (equal); Validation (equal); Visualization (equal); Writing – original draft (equal); Writing – review and editing (equal).

DATA AVAILABILITY

The data that support the findings of this study are available from the corresponding author upon reasonable request.

REFERENCES

[1]O. R. Bilal, R. Süsstrunk, C. Daraio, and S. D. Huber, "Intrinsically polar elastic metamaterials," Adv. Mater. **29**, 1700540 (2017).

[2]A. Palermo, P. Celli, B. Yousefzadeh, C. Daraio, and A. Marzani, "Surface wave non-reciprocity via time-modulated metamaterials," J. Mech. Phys. Solids **145**, 104181 (2020).

[3]X. Hou and V. V. Silberschmidt, "Metamaterials with negative Poisson's ratio: A review of mechanical properties and deformation mechanisms," in *Mechanics of Advanced Materials: Engineering Materials*, edited by V. Silberschmidt and V. Matveenko (Springer, Cham, 2015).

[4]R. Graciá-Salgado, V. M. García-Chocano, D. Torrent, and J. Sánchez-Dehesa, "Negative mass density and ρ-near-zero quasi-two-dimensional metamaterials: Design and applications," Phys. Rev. B **88**, 224305 (2013).

[5]H. Huang, C. Sun, and G. Huang, "On the negative effective mass density in acoustic metamaterials," Int. J. Eng. Sci. **47**, 610–617 (2009).

[6]T. Klatt and M. R. Haberman, "A nonlinear negative stiffness metamaterial unit cell and small-on-large multiscale material model," J. Appl. Phys. **114**, 033503 (2013).

[7]J. Li, X. Wen, and P. Sheng, "Acoustic metamaterials," J. Appl. Phys. **129**, 171103 (2021).

[8]Y. Wang and R. Lakes, "Composites with inclusions of negative bulk modulus: Extreme damping and negative Poisson's ratio," J. Compos. Mater. **39**, 1645–1657 (2005).

[9]W. Yang, Z.-M. Li, W. Shi, B.-H. Xie, and M.-B. Yang, "Review on auxetic materials," J. Mater. Sci. **39**, 3269–3279 (2004).

[10]K. E. Evans and A. Alderson, "Auxetic materials: Functional materials and structures from lateral thinking!," Adv. Mater. **12**, 617–628 (2000).

[11]A. Bezazi, W. Boukharouba, and F. Scarpa, "Mechanical properties of auxetic carbon/epoxy composites: Static and cyclic fatigue behaviour," Phys. Status Solidi (B) **246**, 2102–2110 (2009).

[12]Q. Chen and N. M. Pugno, "In-plane elastic buckling of hierarchical honeycomb materials," Eur. J. Mech.-A/Solids **34**, 120–129 (2012).

[13]O. R. Bilal, D. Ballagi, and C. Daraio, "Architected lattices for simultaneous broadband attenuation of airborne sound and mechanical vibrations in all directions," Phys. Rev. Appl. **10**, 054060 (2018).

[14]W. Elmadih, D. Chronopoulos, and J. Zhu, "Metamaterials for simultaneous acoustic and elastic bandgaps," Sci. Rep. **11**, 14635 (2021).

[15]A. Hosseinkhani, D. Younesian, M. Ranjbar, and F. Scarpa, "Enhancement of the vibro-acoustic performance of anti-tetra-chiral auxetic sandwich panels using topologically optimized local resonators," Appl. Acoust. **177**, 107930 (2021).

[16]N. Aravantinos-Zafiris, N. Kanistras, and M. M. Sigalas, "Acoustoelastic phononic metamaterial for isolation of sound and vibrations," J. Appl. Phys. **129**, 105108 (2021).

[17]G. Li, Y. Chen, W. Chen, J. Liu, and H. He, "Local resonance–Helmholtz lattices with simultaneous solid-borne elastic waves and air-borne sound waves attenuation performance," Appl. Acoust. **186**, 108450 (2022).

[18]A. Farouk and S. Maged, "Acoustic metamaterial for simultaneous noise filtering and energy harvesting from ambient vibrations," in *2021 International Mobile, Intelligent, and Ubiquitous Computing Conference (MIUCC)* (IEEE, 2021), pp. 149–154.

[19]N. J. Gerard, M. Oudich, Z. Xu, D. Yao, H. Cui, C. J. Naify, A. Ikei, C. A. Rohde, X. R. Zheng, and Y. Jing, "Three-dimensional trampolinelike behavior in an ultralight elastic metamaterial," Phys. Rev. Appl. **16**, 024015 (2021).

[20]V. Ramakrishnan and M. J. Frazier, "Acoustic metamaterials with independently tunable mass, damping, and stiffness," J. Acoust. Soc. Am. **151**, A96 (2022).

[21]A. Alderson and K. Alderson, "Auxetic materials," Proc. Inst. Mech. Eng., Part G **221**, 565–575 (2007).

[22]R. H. Baughman, J. M. Shacklette, A. A. Zakhidov, and S. Stafström, "Negative Poisson's ratios as a common feature of cubic metals," Nature **392**, 362–365 (1998).

[23]M. N. Ali and I. U. Rehman, "An auxetic structure configured as oesophageal stent with potential to be used for palliative treatment of oesophageal cancer; Development and *in vitro* mechanical analysis," J. Mater. Sci.: Mater. Med. **22**, 2573–2581 (2011).

[24]X. Ren, R. Das, P. Tran, T. D. Ngo, and Y. M. Xie, "Auxetic metamaterials and structures: A review," Smart Mater. Struct. **27**, 023001 (2018).

[25]Z. Yang, H. Dai, N. Chan, G. Ma, and P. Sheng, "Acoustic metamaterial panels for sound attenuation in the 50–1000 Hz regime," Appl. Phys. Lett. **96**, 041906 (2010).

[26]J. Mei, G. Ma, M. Yang, Z. Yang, W. Wen, and P. Sheng, "Dark acoustic metamaterials as super absorbers for low-frequency sound," Nat. Commun. **3**, 756 (2012).

[27]Y. Xiao, J. Wen, and X. Wen, "Sound transmission loss of metamaterial-based thin plates with multiple subwavelength arrays of attached resonators," J. Sound Vib. **331**, 5408–5423 (2012).

[28]F. Ma, J. H. Wu, M. Huang, W. Zhang, and S. Zhang, "A purely flexible light-weight membrane-type acoustic metamaterial," J. Phys. D: Appl. Phys. **48**, 175105 (2015).

[29]W. Ding, D. Tang, Y. Liu, L. Chen, and X. Sun, "Compact and low crosstalk waveguide crossing using impedance matched metamaterial," Appl. Phys. Lett. **96**, 111114 (2010).

[30]O. R. Bilal, C. H. Yee, J. Rys, C. Schumacher, and C. Daraio, "Experimental realization of phonon demultiplexing in three-dimensions," Appl. Phys. Lett. **118**, 091901 (2021).

[31]D. Torrent and J. Sánchez-Dehesa, "Acoustic metamaterials for new two-dimensional sonic devices," New J. Phys. **9**, 323 (2007).

[32]S. A. Cummer and D. Schurig, "One path to acoustic cloaking," New J. Phys. **9**, 45 (2007).

[33]W. Setyawan and S. Curtarolo, "High-throughput electronic band structure calculations: Challenges and tools," Comput. Mater. Sci. **49**, 299–312 (2010).